Acta Technica *62* (2017), No. 5A, 897–908

Study on the optimum technological parameters of laser cladding applied to hydraulic prop

Bin Liu[2], Meimei Zhang[2], Xiaofeng Li[2,3], Heping Liu[2], PeikangBai[2]

Abstract. In this paper, Fe-based composite coatings were fabricated by laser cladding on 45# steel substrate. The comprehensive effects of different parameters on the properties were studied. Results indicated that the coatings were mainly consisted of [Fe-Ni], Fe-Cr, Co_3Fe_7, $Fe_{0.6}Cr_{1.7}Ni_{1.2}Si_{0.2}Mo_{0.1}$, Cu_9Al_4. The microstructure and hard particle were both critical to improve the properties even with the same original powder. Compared with the substrate, the hardness and corrosion resistance were enhanced obviously. The optimum parameters were identified as??E_S=7.91KJ/cm^2, P=1900W, V=6mm/s, which can not only attained the best properties but also realized faster cladding efficiency.

1. Introduction

Laser processing is a relatively advanced technique for processing materials by means of the interaction of laser beams with components. As one of the practical methods in the filed of manufacturing, laser cladding is a technical process to improve the substrate properties of corrosion resistance, heat-resisting, wear and oxidation behaviors and etcetera in this way. As an advanced surface strengthening process, laser cladding is widely used in automobile manufacturing, mold repair, mining equipment and other industries. Compared with the traditional process, such as surfacing, spraying and plasma spraying, it has the advantages of small deformation of work pieces, high automation and little pollution.

[1]Acknowledgement - The research was financially supported by the Key Research and Development Program of Shanxi Province(No.201603D121002-2), School Foundation of North University of China, Science and Technology Innovation Project of Shanxi Province (No.2016156), China Postdoctoral Science Foundation(No.2016M590214), and the Natural Science Foundation of Shanxi Province, China (No. 2015011036).

[2]Workshop 1 - School of Materials Science and Engineering, North University of China, Taiyuan 030051, China

[3]Corresponding author: Xiaofeng Li; e-mail: lxf@nuc.edu.cn

Fe-based alloy powders are widely used in virtue of their contain certain carbon content, which can react with Cr and other elements to form hard phases, on the other hand, this compound metal surface hardness is changeable and low in price[1]. Hence, there is a certain significance to research on laser cladding of Fe-based alloy powder. Weng.et.al[2]. usedFe-base self-fluxing to repair the V-grooves on ductile cast iron substrate with diode laser cladding technique. Manna, et.al[3]. have made an attempt to explore deposition of Fe-based amorphous/glassy layer on a plain carbon (AISI 1010) steel by laser surface cladding (LSC) ,and improved wear and corrosion resistance of the substrate significantly. Zhanget. al[4] investigated the in situ TiC-VC reinforced Fe-based cladding layer on low carbon steel surface with Fe-Ti-V-Cr-C-CeO_2 alloy powder by laser cladding, they attained a good cladding layer without defects such as cracks and pores, while the hardness and wear resistance of the coatings were 16.85 and 9.06 times than that of the substrate respectively.Nevertheless, most of the previous researches in the respect of Fe-based alloy powder have focused on the analysis of the effect of the cladding of the sample or some parts, the work both on improving the cladding efficiency and effect in practical applications has not been fully explored.

In this paper, as common materials used as hydraulic prop, 45# steel was chosen as the substrate to be cladded with Fe-based alloy powder, the effect of Fe-based alloy powder on the surface quality of cladding material under different process conditions and laser specific energy was investigated, the reference properties include the microstructure of combination status between the cladding layer and the substrate, the change of surface micro-hardness and corrosion resistance of cladding layer.

2. Experimental

Laser cladding was performed on a high-power fiber coupled semiconductor laser processing system (LDF 4000-100) equipped with a powder delivery device[5]. The output power of the equipment is as high as 4.4KW, which can greatly improve the processing efficiency. Laser cladding was carried out adopting a 4mm circular laser spot with a coaxial feeder. Meanwhile, Ar gas was transferred during the process to prevent the samples being oxidized, air compressor was used to cooling and protect the laser head. During the cladding process, laser beam diameter was kept constant with a spot of 4mm. Schematic diagram of laser cladding process can be seen in Fig.1.45# steel (Si:0.27 , Mn: 0.59 , P: 0.12 , C: 0.44, S: 0.03 , balance Fe) was used as the substrate with a dimension of 12mm×10mm×5mm, the samples were polished using abrasive paper and purified by ethyl alcohol prior to their claddind. The composition of the cladding powder was listed in Tab.1. Before the detection, the samples were cut along the direction perpendicular to the laser scanning ensuring that the cross section of the coating is exposed to the surface. Phase composition of the Fe-based alloy coatings were tested with X-ray diffractometer. Different zone and lines of coatings from the point of view of microstructure were evaluated using energy dispersive spectroscopy (EDS). The microstructure and morphology were observed using metallurgical microscope (Axio Scope.A1) and scanning electron microscope (SEM, SU5000). For the investigation of microhardness and corrosion

resistance, Vickers (TMHVS-1000ZVicher's) and electrochemical workstation were used respectively. During the research on corrosion resistance of coatings, specimens were measured in 3.5 wt% NaCl solution at room temperature.

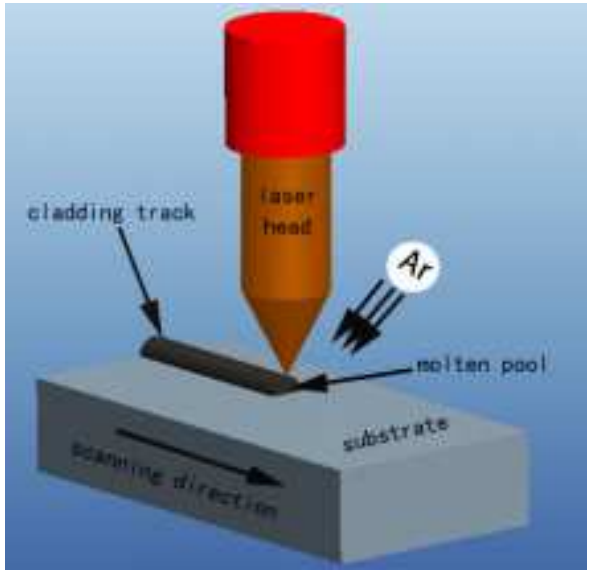

Fig. 1. Sketch map of laser cladding process

Table 1. Composition of the Fe-based alloy powder

Element	C	S	Cr	Ni	Mn	Mo	Si	Co	Cu	Al	Fe
Fe-based powder	0.15	0.01	18.42	8.8	0.31	1.8	0.01	0.14	0.035	0.04	bal.

The laser specific energy (E_s) of the specimens were calculated by the Eq.(1). The aim was to explore the optimum technological parameters and the higher cladding efficiency under the premise of industrial application for hydraulic prop, then we used the picked parameters to make multi-layer lap cladding on the hydraulic prop to confirm the effectiveness of our test. The parameters chosen for the laser cladding process were listed in Tab.2.

$$E = \frac{P}{VD} \tag{1}$$

where P is the laser power (W), V is the scanning speed(mm/s), D is the spot diameter (mm).

Table 2. The parameters for laser cladding process

Specimen number	Laser power(W)	Scanning speed(mm/s)	Laser specific energy(KJ/cm^2)	Spot diameter(mm)
1	2100	2	26.25	4
2	2100	4	13.12	
3	2300	6	9.58	
4	2100	6	8.75	
5	1900	6	7.91	
6	1300	6	5.41	
7	2100	15	3.50	
8	2100	20	2.62	

3. Results and Discussion

3.1. Microstructure analysis

Fig.2 shows micrograps of coatings under different parameters. The different micrographs of eight sets of specimens revealed that the good metallurgical bond was achieved between the cladding layer and the substrate due to the existence of bright white long bands situated the coating and substrate. It should be noted that when the laser specific energy were 3.50 and 2.62, obvious cracking occurred in the dendrite region of the cladding layer, and of which latter crack was more severe than that of the former. This phenomenon was probably attributed to the combined action of the less specific energy and rapid change in temperature of cladding layer. In sum, the specimens of No.7 and No.8 were not suitable for the needs of practical applications.

Fig.3 shows the SEM image and constitution diagram of the optical coating, it exhibited typical rapid solidification microstructure characteristics: transition of columnar cellular crystal perpendicularly along the interface, thick dendritic columnar crystal, fine equiaxed grains and small cellular structure revealed visibly from the bonding interface to the top area of claddded layer. This was conducted to the different solidification cooling rate of different areas in coatings. The higher the cooling rate, the shorter the solidification time, the finer the cellular or dendritic structure becomes. So the cellular crystal and cellular dendritic crystal were fabricated in this area, where the solidification and cooling rate were relatively higher simultaneously. However, the rapid was gradually diminished from the central area of the coating to the top area, of which grain structure was relatively large. In particular, large gradient emerged from the heat conduction between the substrate and cladding layer, consequently, columnar crystals formed vertically along the interface.

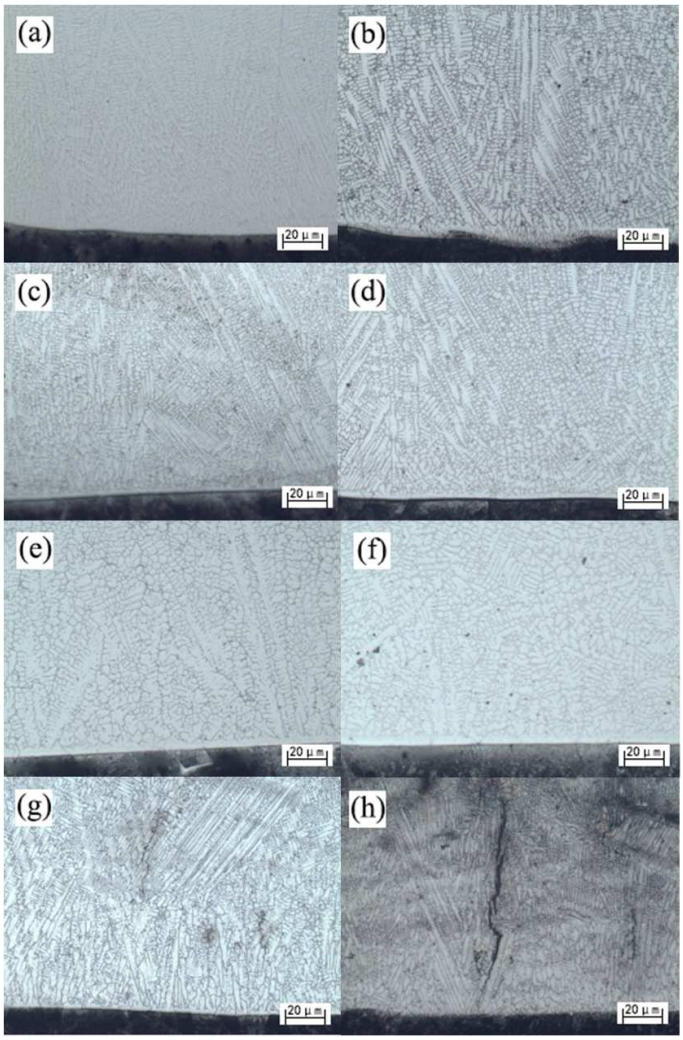

Fig. 2. Micrograps of coatings under different parameters: (a) No.1; (b) No.2; (c) No.3; (d) No.4; (e) No.5; (f) No.6; (g)No.7; (h)No.8

3.2. Phase composition

Fig.4 represents the XRD patterns of the Fe-based coatings. The phase of the cladded layer are [Fe-Ni] Fe-Cr Co_3Fe_7 $Fe_{0.6}Cr_{1.7}Ni_{1.2}Si_{0.2}Mo_{0.1}$ Cu_9Al_4 which indicated that the active element Ni combined with Fe in the powders forming [Fe-Ni] compounds during the cladding process. Besides, Fe, Cr compounds formed in terms of the reactions of Fe, Cr, as the common compounds and phase for thermal spraying, they were conductive to improve the properties of wear resistance and corrosion resistance.

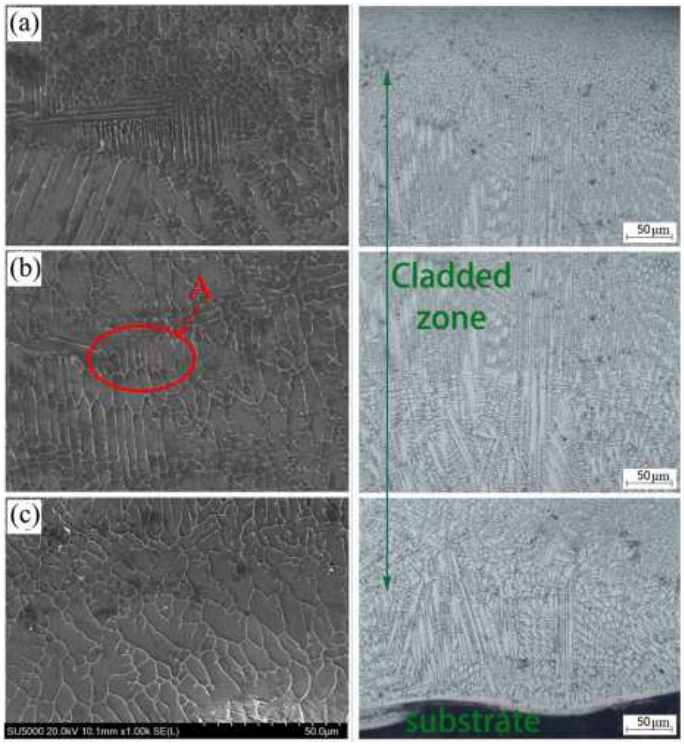

Fig. 3. Optical micrographs of the transverse section of sample No.3: (A) the top area of the cladded layer; (B) the central area of the cladded layer; (C) the bottom area of the cladded layer

By contrast to the spot scanning energy spectrum analysis were shown in Fig.5 and EDS results listed in Tab.3. Thecontent (wt.%) of Cr Mo, Si Al Cu in area B(dendrite region) were higher than that of area A (intergranular region),whichwas considered there were $Cu_9Al_4$and large amounts of $Fe_{0.6}Cr_{1.7}Ni_{1.2}Si_{0.2}Mo_{0.1}$deposited in area B from the observation of XRD results. Based on the previous studies[9], it was concluded that the solid solubility of Fe and Cr is mainly deposited in the dendrite region, which can further explained the integration phenomenon of Fe-Ni Fe-Cr Co_3Fe_7in area A of Fig.3. Therefore, the difference between dendrite region and intergranular region was not only embodied in morphology, but also in constituents. In this process, we had not identify severe component segregation, which can be attributed to the emergence of Marangonicconvection,of which mechanism was as follows: in the process of laser cladding, affected by the combined action of shear stress and buoyancy caused by the gradient of the surface tension in the weld pool, the solution in the bath interior and surface migrated, thus convection current formed. Owing to the convection current, the liquid composition in the bath was homogenized, while the dendrite tip broke accompanied by the grain refined, accordingly the segregation of alloy was obviously decreased in distance and magnitude.

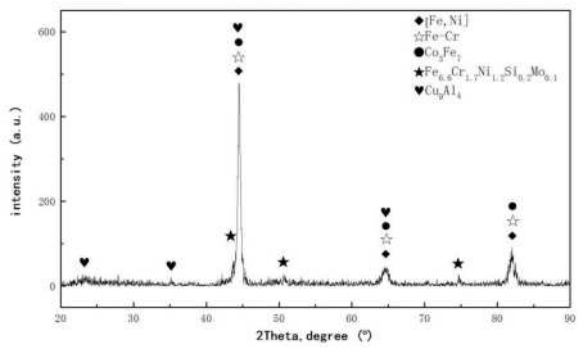

Fig. 4. XRD pattern of cladded layer

Combining with the line scanning energy spectrum analysis of cladding layer as shown in Fig.5, it is obvious to find that the main components in the cladding layer are Fe and Cr compounds, because of which diffraction peak were apparently higher than others. This could be explained by the EDS results of some typical points in the coatings as listed in Tab.3, of which large weight percentage represented in the powder .

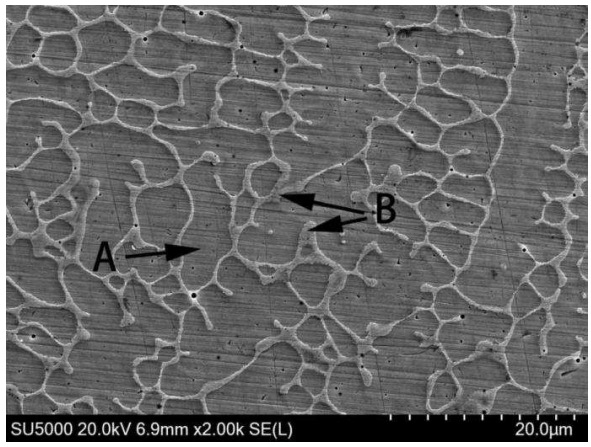

Fig. 5. Spot scanning energy spectrum analysis of cladding layer

Table 3. EDS results of some typical points in the coatings

		C K	SiK	MoL	CrK	MnK	FeK	CoK	NiK
A area	Weight %	7.65	0.29	0.45	10.58	0.45	72.77	0.68	5.59
	Atomic %	27.67	0.46	0.20	8.84	0.35	57.20	0.50	4.14
B area	Weight %	7.93	0.39	2.05	13.74	0.50	67.22	0.70	5.32
	Atomic %	27.90	0.58	0.90	11.17	0.38	53.78	0.50	3.83

3.3. Microhardness

The microhardness distribution of the cladding coatings under different process parameters is illustrated in Fig.6. The results indicated that the hardness of coatings were obviously higher than the substrates, the values were roughly three times than the substrate, of which average value was 550-600$HV_{0.2}$,which was attributed to the presence of reinforcements in the Fe-based coating. It was found that variation tendency of microhardness changes showed similarity under different parameters: higher in the cladded coatings while decreased in the substrate. Which can be contributed to that the cooling rate of cladded layer is decreased with the distance to surface during the cladding process. It is worth noting that the average hardness of the cladding layer increased with the increase of laser specific energy roughly.With the existence of a certain amount of Cr in the original powder, the reinforcement of solid solution produced on the coating during the laser cladding process. Besides, with the great temperature gradient deriving from the course of rapid heating and cooling, fine structures such as crystalline and equiaxed grains distributed in coatings, they were favourable to improve the mechanical properties of coatings. Combining with the EDS results (Fig. 5 and Table.3), the dendrites could be identified as $Fe_{0.6}Cr_{1.7}Ni_{1.2}Si_{0.2}Mo_{0.1}$and Cr_3C_2.

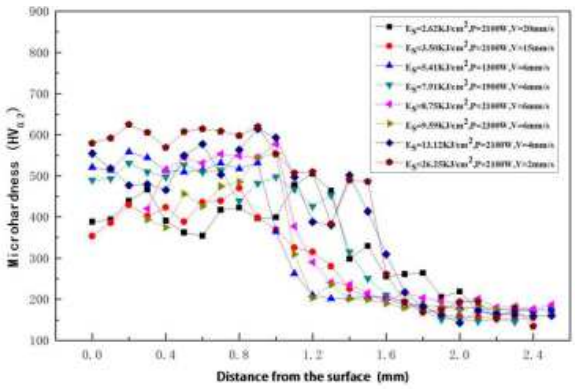

Fig. 6. Microhardness distribution of the cladding coatings under different process parameters

3.4. Corrosion resistance

Fig.7 shows the polarization curves of Fe-based coatings of No.1-8 specimens and the substrate immersed in 3.5wt.%NaCl,whether coatings or the substrate, the curve trend was analogous. However, corrosion resistance of coatings under different parameters were variant. From the Tafel curves, we observed that the potential peak of the coatings of No.2,No.3,No.6,No.8 were all lower than that of substrate, which indicated that the corrosion resistance of these did not improved. This was becauseamounts of Fe included in powders, which were detrimental to the improvement of corrosion resistance.

On the contrary, containing the same compositions of No.1,No4,No.5,No.7coatings showed the higher value of potential than substrates. Combining with the microstucture results, these 4 group coatings possessed more compact microscopic structure and less composition segregation, which made the distribution of Cr,Ni,Al more uniformity. Among these elements, Ni was helpful to enhance the thermodynamic stability of the alloy and greatly improve the corrosion resistance of the reducing medium in the cladding, while as an element with high passivation ability, Cr could improve the passivation ability of coating, thus enhancing the corrosion resistance of coatings. It was worth mentioning that despite No.7 (E_S=3.50KJ/cm2,P=2100W,V=15mm/s) coating showed higher corrosion potential and better corrosion resistance, considering to its crack existed in the cladded layer, which was not suitable for the practical application, further research on it was not considered.

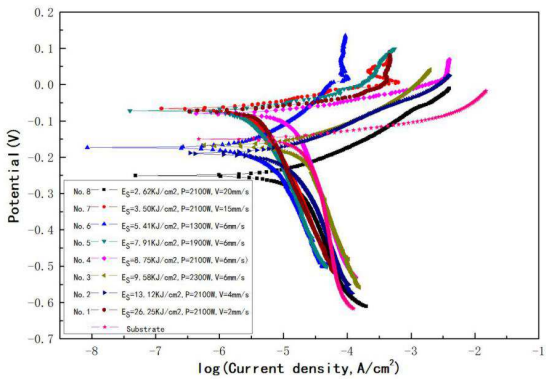

Fig. 7. Polarization curves of Fe-based coatings of No.1-8 specimens and the substrate

After fitting the electrical polarization curve of the No.1,No.4,No.5 specimens, the data were obtained by Tafel shown in Tab.4. According to the fitting results, the self corrosion potential of the three sets of specimens moved about 70-80mV relative to the substrate, which indicated that their corrosion resistance were much better than that of substrates. The major reason was the fabrication of the amorphous phase in the coating ,which possessed excellent corrosion resistance. On the other hand, the effect of alloy strengthening and fine grain strengthening made the corrosion resistance of coating improved to a certain extent. Last but not the least,

Cr_2O_3 was formed in the coating, which could effectively prevent further corrosion of the coating. By contrast with other Ecorr and Icorr of coatings, the No.5 coating (ES=7.91KJ/cm2,P=1900W, V=6mm/s) showed the best corrosion resistance, of which Eccor was maximal (-73.4mV) while the Iccor was relatively lower (1.8412A/cm^2). The disordered grain boundary dislocation was useful to form the continuous protective passivation film.

Table 4. Electrochemical polarization parameters for coatings of No. and substrate

Number of specimens/E_S(KJ/cm^2)	Ecorr (V)	Icorr (A/cm^2)
No.1/E_S=26.25	-0.0736	3.0696E-06
No.4/E_S=8.75	-0.0809	6.9522E-06
No.5/E_S=7.91	-0.0734	1.8412E-06
Substrate	-0.1519	1.1422E-05

Due to the high scanning speed of the No.4 and No.5 coatings under the premise of their good properties, which was the most important factor in improving the efficiency, so they can satisfy the need of practical production. The morphology of the multi-layer with the chosen parameters on hydraulic prop was illustrated in Fig.8, macroscopically, under the condition of this set of parameters, the surface of hydraulic prop achieved good cladding effect. Besides, the average hardness of the surface measured by hand hardness tester was about 550$HV_{0.2}$, thus the accuracy of the experimental results in this paper was verified.

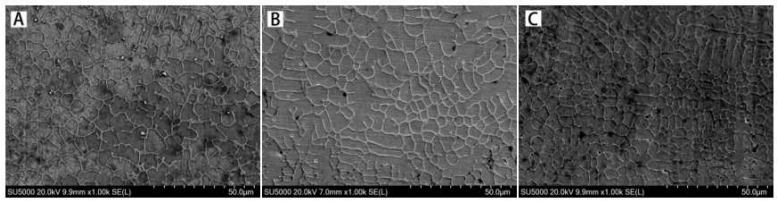

Fig. 8. Micrographs of the central area in different coatings by SEM??(A)the coating of No.1; (B) the coating of No.4; (C) the coating of No.5

4. Conclusions

In this paper, Fe-based composite coatings were fabricated on hydraulic support 45# steel substrate by laser cladding. Results indicated that the coatings mainly consisted of [Fe-Ni], Fe-Cr, Co3Fe7, Fe0.6Cr1.7Ni1.2Si0.2Mo0.1, Cu9Al4, good metallurgical bonding was obtained under the chosen 8 sets of parameters. Compared with the substrate, the coatings showed higher hardness while 3 coatings showed better corrosion resistance than substrate. The parameters were found obviously influencing the properties such as microstructure, hardness and corrosion resistance

of the cladding layer, of which hardness was 3 times higher than substrate and the self corrosion potential was better than that of 70-80mV. This can be conductive to the existence of Cr oxide and the existence of $Fe_{0.6}Cr_{1.7}Ni_{1.2}Si_{0.2}Mo_{0.1}$ Cu_9Al_4. In conclusion, we chose the the specimens of No.4 and No.5(No.4: ES=8.75KJ/cm2, P=2100W, V=6mm/s; No.5: ES=7.91KJ/cm2, P=1900W, V=6mm/s) with higher cladding efficiency and effect as the optimum parameters.

References

[1] X. Yang, X. Peng, J. Chen, F. Wang: *Effect of a small increase in the Ni content on the properties of a laser surface clad Fe-based alloy.* Applied Surface Science *253* (2007), No. 9, 211–220.

[2] Z. Weng, A. Wang, Y. Wang, D. Xiong, H. Tang: *Diode laser cladding of Fe-based alloy on ductile cast iron and related interfacial behavior.* Surface & Coatings Technology *286* (2016), No. 4, 257–262.

[3] I. Manna, J. D. Majumdar, B. R. Chandra, S. Nayak, N. B. Dahotre: *Laser surface cladding of Fe–B–C, Fe–B–Si and Fe-BC-Si-Al-C on plain carbon steel.* Surface & Coatings Technology *201* (2006), Nos. 1–2, 171–180.

[4] H. Zhang, Y. Zou, Z. Zou, D. Wu: *Effect of butt joint gap to high strength automobile steel of fiber laser welding.* Optics & Laser Technology *65* (2015), No. 12, 41–52.

[5] G. Chen, F. Chen, Y. Zhang, S. Li, B. Kang: *Thermal deflection of an inverse thermoelastic problem in a thin isotropic circular plate.* Chinese Journal of Lasers *38* (2011), No. 6, 797–804.

[6] H. Yang, X. Lin, W. Huang, J. Li, Y. Zhou: *The influences of processing parameters on forming characterizations during laser rapid forming.* Materials Science & Engineering A *360* (2003), Nos. 1–2, 521–528.

[7] A. Emamian, S. F. Corbin, A. Khajepour: *The influence of combined laser parameters on in-situ formed TiC morphology during laser cladding.* Surface & Coatings Technology *206* (2011), No. 1, 124–131.

[8] J. Sampedroa, I. Péreza, B. Carcela, J. A. Ramosa: *Laser Cladding of TiC for Better Titanium Components.* Physics Procedia *12* (2011), No. 12, 198–210.

[9] C. Yao, J. Huang, P. Zhang, Z. Li, Y. Wu: *Toughening of Fe-based laser-clad alloy coating.* Applied Surface Science *257* (2011), No. 6, 587–606.

[10] M. Aghasibeig, H. Fredriksson: *Laser cladding of a featureless iron-based alloy.* Surface & Coatings Technology *209*, (2012), No. 38, 264–275.

Received November 16, 2017